VOL. 9, NO. 8, AUGUST 2014 ISSN 1819-6608
ARPN Journal of Engineering and Applied Sciences


www.arpnjournals.com

PRESSURE AND PRESSURE DERIVATIVE ANALYSIS FOR TRIPLE-POROSITY AND SINGLE-PERMEABILITY SYSTEMS IN NATURALLY FRACTURED VUGGY RESERVOIRS

Freddy Humberto Escobar, Raul Fernando Rojas and Juan Diego Rojas
Universidad Surcolombiana/CENIGAA, Avenida Pastrana - Cra 1, Neiva, Huila, Colombia
E-Mail: fescobar@usco.edu.co

ABSTRACT

There are several developed models in the literature to interpret pressure tests in heterogeneous reservoirs; however, none of these had developed a methodology able to estimate the characteristic parameters of triple-porosity and single-permeability reservoirs without storage and wellbore damage. Amacho *et al.* (2005) analytical solution was used as a reference point for modeling the complexity of these reservoirs. Since none commercial software includes this analytical solution up to now, then, this proposal represents the characterization of heterogeneous naturally fractured vuggy reservoirs by extending the *TDS* methodology which refers to the "fingerprints" found on the pressure and pressure derivative versus time curve -without using type-curve matching- during the transient flow period and dominated flow boundaries. This leads to obtain the dimensionless storativity coefficients, ω_v and ω_f for the systems of fractures and vugs and, also, the interporosity flow parameters: matrix - fracture, matrix - vugs, fractures - vugs, λ_{mf}, λ_{vf}, y λ_{mv}. The mathematical expressions proposed were verified successfully by simulating synthetic pressure tests, in which there were found very good adjustments between the calculated results and the values used for simulations. Although, one filed case was worked, the agreement was not so good since part of the input data was assumed.

Keywords: interporosity flow parameters, storativity coefficients, vuggy reservoirs, naturally fractured systems.

1. INTRODUCTION

Recent studies have shown that the presence of cavities or vugs in naturally fractured carbonate reservoirs affect the well-pressure behavior since they present a complex porous system identified as a triple-porosity naturally-fractured reservoir. As a consequence, strange anomalies are observed in the slope of the semilog plot during the transition period. The behavior of the dimensionless pressure versus dimensionless time has an alteration of the normal slope reflected as an additional depression in the curve. These abnormalities in the slope changes are caused by the presence of an additional pore system with different petrophysical properties in the reservoir due to the presence of fractures, vugs and matrix, or large fractures, small fractures and matrix, which is especially present in naturally fractured carbonate reservoirs.

From the years 60s to now, there have been various formulations to conceptualize naturally fractured formations and to establish the fluid flow modeling in this type of rocks. Initially, dual-porosity models were proposed; the most used in the oil industry to present a better field-scale application is the one developed by Warren and Root (1963). It is classified as a dual-medium formulation (double-porosity model) in which the fractures form a network of channels providing fluid flow parallel to the main permeability axi and the matrix subsystem is constituted for a discrete homogeneous and isotropic blocks, providing the capacity of storage. These dual-medium formulations were also applied to characterize triple-porosity systems, where the presence of vugs was calculated as part of the fractures system or as part of the matrix system, simplifying the calculations. However, this assumption did not correctly describe the fluid mechanics behavior in the reservoir, because vugs and matrix do not have the same effect or interaction with the fracture network. Taking into account the limitations of these models, different authors have reformulated the theoretical principles to try to establish a model that captures the reality of the process flow taking place in triple porosity reservoirs.

Abdassah and Ershaghi (1986) presented a triple porosity model and unique permeability. They considered a model for unsteady flow between the system of fractures, with two types of matrix blocks, and only the primary flow through the fracture system. Also, they considered the existence of parallel flow between the fracture system, with homogeneous properties, and the interaction with two separate groups of matrix blocks having different permeabilities and porosities.

Cols and Rodríguez (2004) developed an analytical solution for characterizing secondary porosity in naturally fractured reservoirs. They generated a nested triple-porosity and single-permeability model for transient pressure of a well producing in a naturally fractured reservoir. It was considered as a triple-porosity system acting at different scales: matrix, secondary porosity of small and large scale, where the fluid flow through these media takes place in series: the matrix exchanges fluids with the small-scale secondary porosity which also feeds the large-scale secondary porosity.

Wu and Cols (2004) proposed a conceptual model of triple porosity and triple permeability. They conceptualized the fracture-matrix system formed by a matrix and two types of fractures: large and small fractures; and extended the concept of dual permeability by adding a connection (with small fractures), between the large fractures and matrix blocks.

Camacho *et al*. (2005) presented a study to model secondary porosities, mainly naturally fractured vuggy carbonate reservoirs. This model utilized the approximation of pseudosteady interporosity flow (it means that the fluid transfer among the matrix, the vugs and fractures is directly proportional to the difference of the average pressure in volume with the macroscopic matrix, fractures and vugs). They proposed solutions to two different cases: the first one, when no primary flow occurs through vugs, which is an extension of the model of Warren and Root (1963), and the second one, where the dissolution process has created an interconnected system of vugs. In both cases, there exists an interaction between the matrix, the vugs and fracture system. Based on the analytical solution introduced by Camacho *et al*. (2005) and by referring the studies and analysis techniques presented by Escobar *et al*. (2004) and Mirshekari *et al.* (2007) a methodology is developed here to interpret pressure behavior and pressure derivative of the transient flow period and the period of flow dominated by bordering in naturally fractured vuggy carbonate reservoirs; and in that way the dimensionless storativity coefficients and the interporosity flow parameters matrix-fracture, matrix-vugs and vugs-fractures can be estimated. The methodology was successfully tested with synthetic and field examples.

2. MATHEMATICAL DEVELOPMENT

In this study and the work of Rojas and Rojas (2014) an extension of the *TDS* technique, Tiab (1993), was applied to observe the characteristic behavior of the dimensionless pressure and dimensionless pressure derivative versus dimensionless time, by changing the different dimensionless storativity coefficients and interporosity flow parameters, so some expressions to estimate them were developed. The idea is to use the characteristic points, lines and intersection points of several straight-line portions, slopes and starting points, see Figure-1, to correlate their behavior and develop the expressions for the interpretation technique.

The dimensionless pressure and pressure derivative behavior were obtained from the model presented by Camacho *et al*. (2005) which along to several parameter definitions is given in Appendix A.

The dimensionless time, pressure and pressure derivative used for the mathematical development are:

$$t_D = \frac{0.0002637kt}{(\phi c_t)_{m+f+v}\,\mu r_w^2} \quad (1)$$

$$P_D = \frac{kh\Delta P}{141.2q\mu B} \quad (2)$$

$$t_D * P_D' = \frac{kh(t*\Delta P')}{141.2q\mu B} \quad (3)$$

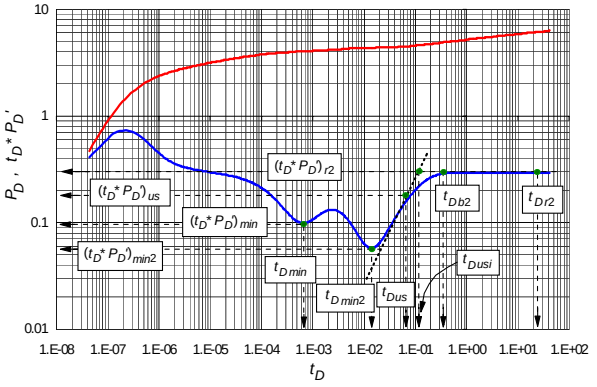

Figure-1. Points or fingerprints characteristic the triple porosity reservoirs.

2.1. Matrix-fracture interporosity flow parameter, λ_{mf}

Figure-2 shows the effect of the matrix-fracture interporosity flow parameter, λ_{mf}, on the behavior of the dimensionless pressure derivative versus dimensionless time for reservoir with triple porosity (naturally fractured vuggy reservoirs) with constant values of $\lambda_{vf}=1\times10^{-7}$, $\lambda_{mv}=1\times10^{-10}$, $\omega_f=1\times10^{-4}$ and $\omega_v=1\times10^{-5}$. The pressure behavior for these conditions is presented in Figure-3.

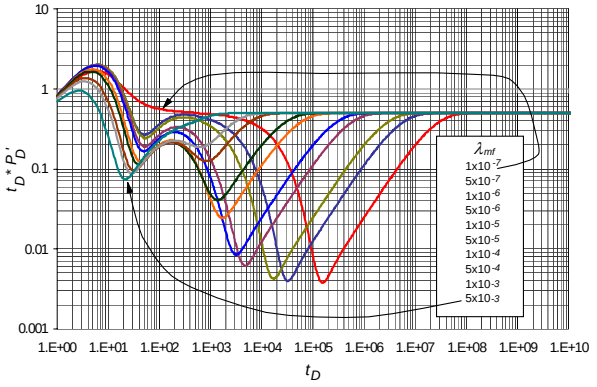

Figure-2. Effect of λ_{mf} on the dimensionless pressure derivative, $\lambda_{vf}=1\times10^{-7}$, $\lambda_{mv}=1\times10^{-10}$, $\omega_f=1\times10^{-4}$ and $\omega_v=1\times10^{-5}$

Basically, this parameter affects the occurrence of the transition period. When the value of λ_{mf} decreases, the presence of the second minimum point, the unit-slope behavior just before the second radial flow (the radial flow formed in the homogenous systems once the transition period is no longer felt) and the same second radial flow occur later. In addition to this, the first transition zone is also affected by this interporosity flow parameter; however, the change is not significant and makes it impractical to use in a correlation.

Figure-3 shows the effects when λ_{mf} decreases. Slope changes are better appreciated in the pressure curve as a consequence of the typical transitions generated by

the influence of different porous media affecting fluid flow in naturally fractured vuggy reservoirs.

Considering these observations and the points or characteristic fingerprints, the expressions generated to calculate the matrix-fracture interporosity flow parameter are these:

1) Using the second minimum point, P_{Dmin2}/ $(t_D*P_D')_{min2}$ and t_{Dmin2}:

$$\lambda_{mf} = \frac{A}{t_{Dmin2}} + \frac{B}{t_{Dmin2}\ln\left(\frac{P_{Dmin2}}{(t_D*P_D')_{min2}}\right)} + \frac{C}{t_{Dmin2}\left(\ln\left(\frac{P_{Dmin2}}{(t_D*P_D')_{min2}}\right)\right)^2} + \frac{D}{t_{Dmin2}\left(\ln\left(\frac{P_{Dmin2}}{(t_D*P_D')_{min2}}\right)\right)^3} + \frac{E}{t_{Dmin2}\left(\ln\left(\frac{P_{Dmin2}}{(t_D*P_D')_{min2}}\right)\right)^4} + \frac{F}{t_{Dmin2}\left(\ln\left(\frac{P_{Dmin2}}{(t_D*P_D')_{min2}}\right)\right)^5} \quad (4)$$

The constants used in Equation (4) are given in Table-1.

Table-1. Constants for Equation (4).

Rank λ_{mf}	1×10^{-4} to 1×10^{-3}	1×10^{-5} to 1×10^{-3}	1×10^{-6} to 1×10^{-3}	1×10^{-7} to 1×10^{-3}	1×10^{-8} to 1×10^{-3}
λ_{vf}	1×10^{-4}	1×10^{-5}	1×10^{-6}	1×10^{-7}	1×10^{-8}
λ_{mv}	1×10^{-7}	1×10^{-8}	1×10^{-9}	1×10^{-10}	1×10^{-11}
ω_f	1×10^{-1}	1×10^{-2}	1×10^{-3}	1×10^{-4}	1×10^{-5}
ω_v	1×10^{-2}	1×10^{-3}	1×10^{-4}	1×10^{-5}	1×10^{-6}
A	18.750525	-0.01991929	1.4395861	0.61733522	0.87955429
B	-175.1714	-1.1282632	-33.795176	-14.552994	-21.273956
C	548.95252	9.4026458	311.82424	134.54613	201.21104
D	-559.03426	0	-1436.2235	-635.27347	-955.35918
E	0	0	3438.6978	1667.9363	2413.0321

2) Using the beginning of the second radial flow, t_{Db2}:

$$\lambda_{mf}^{-1} = A + B\times t_{Db2}^{1.5} + \frac{C\times t_{Db2}}{\ln(t_{Db2})} \quad (5)$$

Constant A, B and C are provided in Table-2.

Table-2. Constants for Equation (5).

Constant	Value
A	-122.95071
B	7.3564664×10^{-6}
C	0.9062836

Equation (5) is applicable to $1\times10^{-6}<\lambda_{mf}<1\times10^{-3}$, $1\times10^{-8}<\lambda_{vf}<1\times10^{-4}$, $1\times10^{-11}<\lambda_{mv}<1\times10^{-7}$, $1\times10^{-5}<\omega_f<1\times10^{-1}$ and $1\times10^{-6}<\omega_v<1\times10^{-2}$.

Another expression developed using the beginning of the second radial flow is:

$$\lambda_{mf}^{-1} = A + \frac{B}{t_{Db2}} + \frac{C}{t_{Db2}^2} + \frac{D}{t_{Db2}^3} + \frac{E}{t_{Db2}^4} + \frac{F}{t_{Db2}^5} \quad (6)$$

With constants A through F given in Table-3.

Table-3. Constants for Equation (6).

Constant	Value
A	-4.7766068×10^{-8}
B	12.367255
C	-622407
D	9.0548479×10^{10}
E	-2.7050964×10^{15}
F	2.1249078×10^{19}

The above equation is applicable for the range of $1\times10^{-6} < \lambda_{mf} <1\times10^{-3}$, $1\times10^{-8} <\lambda_{vf}<1\times10^{-4}$, $1\times10^{-11}<\lambda_{mv}<1\times10^{-7}$, $1\times10^{-5}< \omega_f<1\times10^{-1}$ and $1\times10^{-6} < \omega_v<1\times10^{-2}$.

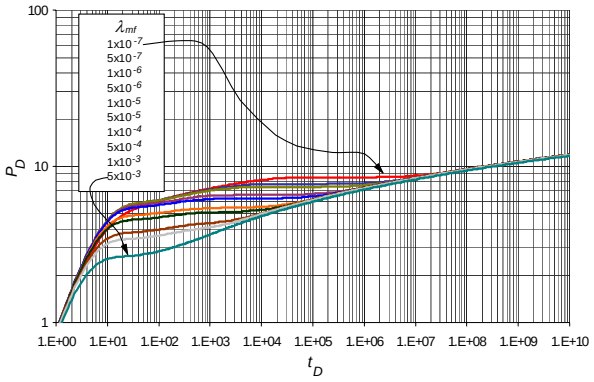

Figure-3. Effect of λ_{mf} on the dimensionless pressure, λ_{vf}=1×10^{-7}, λ_{mv}=1×10^{-10}, ω_f=1×10^{-4} and ω_v=1×10^{-5}.

Table-4. Constants for Equations (7) and (8).

Constant	Value	Value
A	1543.0125	-7517.7246
B	-0.0031036453	-0.043074373
C	348.57011	39.852572
D	-1018.2157	0.48824847
E	-5442.053	8247.468
F	32.722676	121.74982
G	-11958.569	2708.9279
H	494.01527	2249.5118
I	-4460.9516	19002.275

3) Using a time point, t_{Dus}, read on the unit-slope line developed during the transition period before the starting of the second radial flow regime. The pressure derivative is read at a time t_{Dus} which is located one log cycle after the second minimum point, t_{Dmin2}. The equation would be given for λ_{vf} =1×10^{-6}, λ_{mv}=1×10^{-9}, ω_f =1×10^{-3}, ω_v=1×10^{-4} and 1×10^{-6}<λ_{mf} <1×10^{-4}:

$$\ln\left(\lambda_{mf}\right)=A+B\times t_{Dus}^{0.5}+\frac{C}{t_{Dus}^{0.5}}+\frac{D\times\ln\left(t_{Dus}\right)}{t_{Dus}}+ E\times\left(t_D*P_D'\right)_{us}\times\ln\left(\left(t_D*P_D'\right)_{us}\right)+F\times\left(\ln\left(\left(t_D*P_D'\right)_{us}\right)\right)^2 +G\times\left(t_D*P_D'\right)_{us}^{0.5}+H\times\ln\left(t_D*P_D'\right)_{us}+\frac{I}{\ln\left(t_D*P_D'\right)_{us}} \quad (7)$$

For which constants *A* through *I* are given in the second column of Table-4. Also, for λ_{vf}=1×10^{-7}, λ_{mv}= 1×10^{-10}, ω_f=1×10^{-4}, ω_v=1×10^{-5} and 1×10^{-7}<λ_{mf} <1×10^{-4}, the resulting expression is:

$$\ln\left(\lambda_{mf}\right)=A+B\times\left(\ln\left(t_{Dus}\right)\right)^2+\frac{C}{t_{Dusi}^{0.5}}+\frac{D\times\ln\left(t_{Dus}\right)}{t_{Dus}}+E\times\left(t_D*P_D'\right)_{us}^{0.5}\times\ln\left(\left(t_D*P_D'\right)_{us}\right)+F\times\left(\ln\left(\left(t_D*P_D'\right)_{us}\right)\right)^2+G\times\left(t_D*P_D'\right)_{us}^{0.5}+H\times\ln\left(\left(t_D*P_D'\right)_{us}\right)+I\times e^{-\left(t_D*P_D'\right)_{us}} \quad (8)$$

Constants *A* through *I* are given in the third column of Table-4.

4) Another way to use the Equations (7) and (8) is reading the intercept point between the unit-slope line formed at the end of the transition period with the line of the second radial flow regime, taking t_{Dus} as t_{Dusi} and $(t_D*P_D')_{us}$ as $(t_D*P_D')_{usi}$. Since any point on the radial flow has a dimensionless pressure derivative of 0.5 then, at this intersection point, $(t_D*P_D')_{usi}$=0.5, replacing this value and the respective constant, it yields:

$$\ln\left(\lambda_{mf}\right)=A+B\times t_{Dusi}^{0.5}+\frac{C}{t_{Dusi}^{0.5}}+\frac{D\times\ln\left(t_{Dusi}\right)}{t_{Dusi}} \quad (9)$$

For λ_{vf}=1×10^{-6}, λ_{mv}=1×10^{-9}, ω_f=1×10^{-3}, ω_v=1×10^{-4} and 1×10^{-6}<λ_{mf} <1×10^{-4} with constants *A*, *B*, *C* and *D* provided in the second column of Table-5.

Table-5. Constants for Equations (9) and (10)

Constant	Value	Value
A	1082.188281	380.1675508
B	-0.0031036453	-0.043074373
C	348.57011	39.852572
D	-1018.2157	0.48824847

For λ_{vf}=1×10^{-7}, λ_{mv}=1×10^{-10}, ω_f=1×10^{-4}, ω_v=1×10^{-5} and 1×10^{-7}<λ_{mf} <1×10^{-4}.

$$\ln\left(\lambda_{mf}\right)=A+B\times\left[\ln\left(t_{Dusi}\right)\right]^2+\frac{C}{t_{Dusi}^{0.5}}+\frac{D\times\ln\left(t_{Dusi}\right)}{t_{Dusi}} \quad (10)$$

Constants for Equation (10) are given in the third column of Table-5.

2.2. Matrix-vugs interporosity-flow parameter, λ_{mv}

Figure-4 and Figure-5 show the effect of the matrix-fracture interporosity-flow parameter, λ_{mv}, on the transient pressure behavior for constant values of λ_{mf}=1×10^{-7}, λ_{vf}=1×10^{-10}, ω_f=1×10^{-7} and ω_v=1×10^{-8}.

Unlike the observation of λ_{mf}, the starting time of the second radial flow converges at the same point for different λ_{mv} values and unit-slope line at the end of the pressure derivative depression varies in length but it is the same in terms of location (no parallel displacement along the time axis). These observations lead to develop the expressions given below.

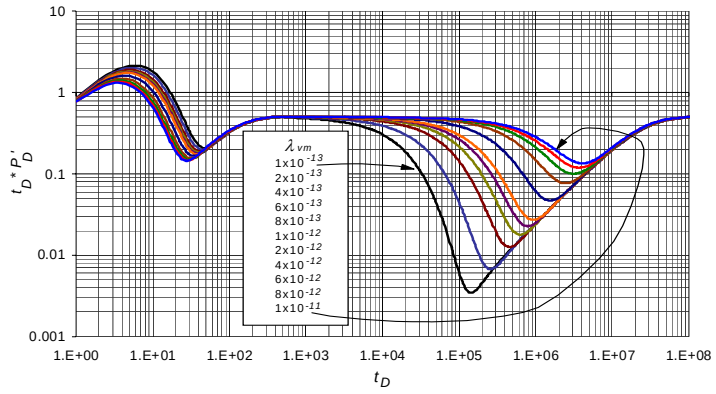

Figure-4. Effect of λ_{mv} on the dimensionless pressure derivative for $\lambda_{mf}=1\times10^{-7}$, $\lambda_{vf}=1\times10^{-10}$, $\omega_f=1\times10^{-7}$ and $\omega_v=1\times10^{-8}$.

5) Using the second minimum point, $P_{Dmin2}/\ (t_D*P_D')_{min2}$ and t_{Dmin2}:

$$\lambda_{mv} = A + B\times\frac{P_{D\min 2}}{(t_D * P_D')_{\min 2}} + \frac{C}{t_{D\min 2}} + \frac{D}{t_{D\min 2}^2} + \frac{E}{t_{D\min 2}^3} + \frac{F}{t_{D\min 2}^4} \qquad (11)$$

The constants depending on λ_{mf}, λ_{vf}, ω_f and ω_v are provided in Table-6.

Table-6. Constants for Equation (11).

Rank λ_{mv}	1×10^{-11} to 1×10^{-8}	1×10^{-12} to 1×10^{-9}	1×10^{-12} to 1×10^{-10}	1×10^{-13} to 1×10^{-11}
λ_{mf}	1×10^{-4}	1×10^{-5}	1×10^{-6}	1×10^{-7}
λ_{vf}	1×10^{-7}	1×10^{-8}	1×10^{-9}	1×10^{-10}
ω_f	1×10^{-4}	1×10^{-5}	1×10^{-6}	1×10^{-7}
ω_v	1×10^{-5}	1×10^{-6}	1×10^{-7}	1×10^{-8}
A	-1.6415236×10^{-9}	-1.4333864×10^{-11}	-1.7301336×10^{-13}	-5.1835462×10^{-16}
B	5.9010132×10^{-14}	8.3945406×10^{-17}	1.2107007×10^{-17}	8.4049346×10^{-21}
C	1.5850872×10^{-7}	1.6214372×10^{-8}	1.7214656×10^{-9}	2.3157263×10^{-10}
D	6.008467×10^{-6}	1.5473226×10^{-6}	1.9670959×10^{-7}	2.610502×10^{-8}
E	9.4481581×10^{-6}	-3.3702849×10^{-5}	-3.5827173×10^{-6}	-5.6665697×10^{-7}
F	0.0019066336	0.0011408245	0.00017086007	3.1146649×10^{-5}

6) Using the dimensionless delta time Δt_D defined as the difference between t_{Dusi} and t_{Dmin2}:

$$\lambda_{mv} = \frac{A}{\lambda_{mf}} + \frac{B\times\Delta t_D}{\lambda_{mf}} + \frac{C\times\Delta t_D^2}{\lambda_{mf}} + \frac{D\times\Delta t_D^3}{\lambda_{mf}} \qquad (12)$$

The constants depending upon λ_{mf}, λ_{vf}, ω_f and ω_v values are given in Table-7.

2.3. Vugs-fractures interporosity flow parameter, λ_{vf}

Figure-6 and Figure-7 show the effect of vugs-fracture interporosity flow parameter λ_{vf} on the behavior of the dimensionless pressure and the dimensionless pressure derivative having constant values of $\lambda_{mf}=1\times10^{-2}$, $\lambda_{mv}=1\times10^{-7}$, $\omega_f=1\times10^{-2}$ and $\omega_v=1\times10^{-3}$.

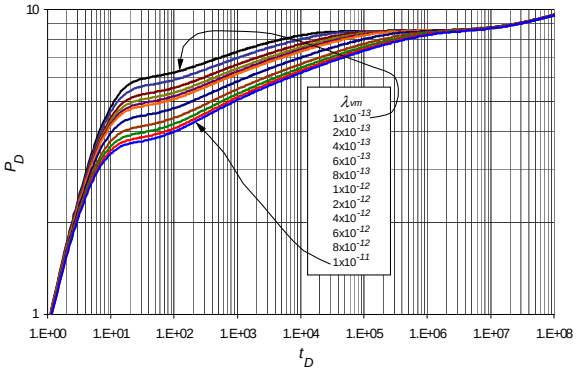

Figure-5. Effect of λ_{mv} on the dimensionless pressure for $\lambda_{mf}=1\times10^{-7}$, $\lambda_{vf}=1\times10^{-10}$, $\omega_f=1\times10^{-7}$ and $\omega_v=1\times10^{-8}$.

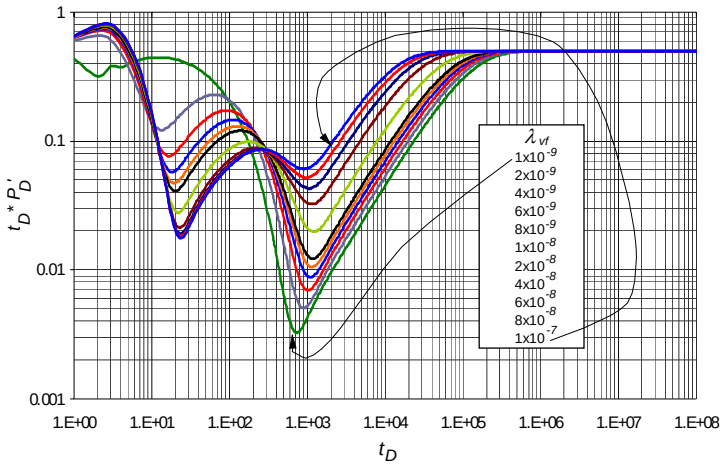

Figure-6. Effect of λ_{vf} on the dimensionless pressure derivative for $\lambda_{mf}=1\times10^{-2}$, $\lambda_{mv}=1\times10^{-7}$, $\omega_f=1\times10^{-2}$ and $\omega_v=1\times10^{-3}$.

Table-7. Constants for Equation (12).

Rank λ_{mv}	**1×10^{-11} to 1×10^{-8}**	**1×10^{-12} to 1×10^{-9}**	**1×10^{-12} to 1×10^{-10}**	**1×10^{-13} to 1×10^{-11}**
λ_{mf}	1×10^{-4}	1×10^{-5}	1×10^{-6}	1×10^{-7}
λ_{vf}	1×10^{-7}	1×10^{-8}	1×10^{-9}	1×10^{-10}
ω_f	1×10^{-4}	1×10^{-5}	1×10^{-6}	1×10^{-7}
ω_v	1×10^{-5}	1×10^{-6}	1×10^{-7}	1×10^{-8}
A	1.0013273×10^{-9}	-1.1127195×10^{-12}	8.3458729×10^{-17}	-2.1318805×10^{-17}
B	-1.510529×10^{-13}	1.6910126×10^{-17}	9.8924541×10^{-22}	4.2037988×10^{-24}
C	7.5990051×10^{-18}	-8.4508641×10^{-23}	-9.1889747×10^{-28}	-2.471287×10^{-31}
D	-1.2747192×10^{-22}	1.3923415×10^{-28}	2.0543111×10^{-34}	4.5497101×10^{-39}

As for the case of λ_{mf}, the variation of the interporosity flow parameter between vugs-fracture, λ_{vf}, has the same effect on the behavior of the dimensionless pressure and the dimensionless pressure derivative. It affects the second minimum point, the onset of unit-slope line occurring previous to the second radial flow regime. The last one occurs later (location of the second depression in the pressure derivative). However λ_{vf} does not alter in the same extent as λ_{mf} does. For example, comparing Figure-6 to Figure-2, the second minimum time point has smaller variation but their corresponding pressure derivative values vary largely with changes of λ_{vf} than λ_{mf}. Based on these considerations, the generated expressions for calculation the interporosity flow parameter between vugs-fractures are as follows:

7) Using the second minimum point, $P_{Dmin2}/(t_D*P_D')_{min2}$ and t_{Dmin2}:

$$\lambda_{vf}=A+\frac{B}{t_{Dmin2}}+C\times\ln\left(\frac{P_{Dmin2}}{(t_D*P_D')_{min2}}\right)+\frac{D}{(t_{Dmin2})^2}+E\times\left(\ln\left(\frac{P_{Dmin2}}{(t_D*P_D')_{min2}}\right)\right)^2+\frac{F\times\ln\left(\frac{P_{Dmin2}}{(t_D*P_D')_{min2}}\right)}{t_{Dmin2}}+\frac{G}{(t_{Dmin2})^3}+H\times\left(\ln\left(\frac{P_{Dmin2}}{(t_D*P_D')_{min2}}\right)\right)^3+\frac{I\times\left(\ln\left(\frac{P_{Dmin2}}{(t_D*P_D')_{min2}}\right)\right)^2}{t_{Dmin2}}+\frac{J\times\ln\left(\frac{P_{Dmin2}}{(t_D*P_D')_{min2}}\right)}{(t_{Dmin2})^2} \quad (13)$$

Constants for Equation (13) are presented in Table-8.

Table-8. Constants for Equation (13).

Rank λ_{vf}	5×10^{-8} to 9×10^{-7}	3×10^{-9} to 3×10^{-8}
λ_{mf}	1×10^{-4}	1×10^{-5}
λ_{mv}	1×10^{-10}	1×10^{-11}
ω_f	1×10^{-4}	1×10^{-5}
ω_v	1×10^{-5}	1×10^{-6}
A	3.7301428×10^{-06}	2.8589362×10^{-06}
B	0.00014429885	0.0064676422
C	2.66054×10^{-06}	-1.5822898×10^{-06}
D	0.21684084	3.6608159
E	6.4429743×10^{-07}	2.9058185×10^{-07}
F	-0.00023134716	-0.0023232953
G	2.9644256	703.42261
H	5.2651235×10^{-08}	-1.7712087×10^{-08}
I	5.4043502×10-05	0.00020931574
J	0.010538647	-0.66612539

For another range:

$$\lambda_{vf}=\frac{A+\left(B\times t_{D\min 2}\right)+\left(C\times\frac{P_{D\min 2}}{\left(t_D*P_D'\right)_{\min 2}}\right)+\left(D\times\left(\frac{P_{D\min 2}}{\left(t_D*P_D'\right)_{\min 2}}\right)^2\right)}{1+\left(E\times t_{D\min 2}\right)+\left(F\times\frac{P_{D\min 2}}{\left(t_D*P_D'\right)_{\min 2}}\right)+\left(G\times\left(\frac{P_{D\min 2}}{\left(t_D*P_D'\right)_{\min 2}}\right)^2\right)} \quad (14)$$

The constants depending on the values of λ_{mf}, λ_{mv}, ω_f and ω_v are given in Table-9.

8) Using unit-slope line developed prior to the second radial flow regime. This point is read with the same conditions as for λ_{mf} estimation. The equation would be:

$$\lambda_{vf}=A+B\times\ln\left(t_{Dus}\right)+C\times\left(\ln\left(t_{Dus}\right)\right)^2+D\times\left(\ln\left(t_{Dus}\right)\right)^3+E\times\left(t_D*P_D'\right)_{us}+F\times\left(\left(t_D*P_D'\right)_{us}\right)^2+G\times\left(\left(t_D*P_D'\right)_{us}\right)^3+H\times\left(\left(t_D*P_D'\right)_{us}\right)^4 \quad (15)$$

With the respective constants given in Table-10.

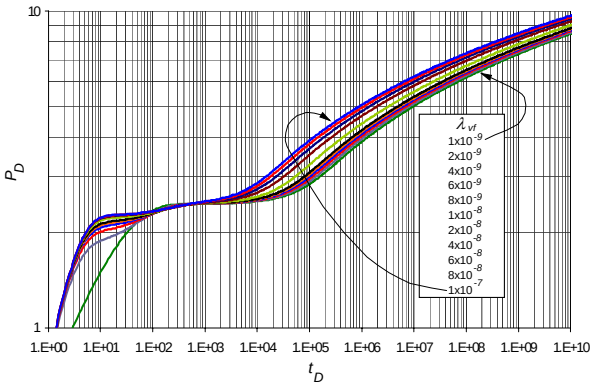

Figure-7. Effect of λ_{vf} on the dimensionless pressure for $\lambda_{mf}=1\times10^{-2}$, $\lambda_{mv}=1\times10^{-7}$, $\omega_f=1\times10^{-2}$ and $\omega_v=1\times10^{-3}$.

Table-9. Constants for Equation (14)

Rank λ_{vf}	1×10^{-9} to 1×10^{-7}	5×10^{-7} to 1×10^{-5}
λ_{mf}	1×10^{-2}	1×10-1
λ_{mv}	1×10^{-8}	1×10-7
ω_f	1×10^{-2}	1×10-1
ω_v	1×10^{-3}	1×10-2
A	-4.6443423×10^{-07}	-3.4145192×10^{-05}
B	8.0324488×10^{-11}	-4.9380799×10^{-08}
C	9.936457×10^{-10}	-5.6541379×10^{-7}
D	-6.2787366×10^{-13}	-9.0007149×10^{-12}
E	0.0010076483	-0.002093633
F	-0.13825481	-0.092186966
G	0.00015750301	-0.0038416544

Table-10. Constants for Equation (15)

Ran λ_{vf}	5×10^{-8} to 9×10^{-7}	3×10^{-9} to 3×10^{-8}
λ_{mf}	1×10^{-4}	1×10^{-5}
λ_{mv}	1×10^{-10}	1×10^{-11}
ω_f	1×10^{-4}	1×10^{-5}
ω_v	1×10^{-5}	1×10^{-6}
A	9.1288254×10^{-5}	4.6546782×10^{-6}
B	-2.7841968×10^{-5}	-1.2091635×10^{-6}
C	2.8397741×10^{-6}	1.0455704×10^{-7}
D	-9.6854292×10^{-8}	-3.0237203×10^{-9}
E	9.0567788×10^{-7}	7.0123633×10^{-7}
F	-3.574932×10^{-6}	-7.8123529×10^{-6}
G	5.1720753×10^{-6}	3.8047196×10^{-5}
H	-2.3694035×10^{-6}	-6.7541516×10^{-5}

For another range:

$$\lambda_{vf}=\frac{A+B\times\ln\left(t_{Dus}\right)+C\times\left(\ln\left(t_{Dus}\right)\right)^2+D\times\ln\left(\left(t_D*P_D'\right)_{us}\right)}{1+E\times\ln\left(t_{Dus}\right)+F\times\left(\ln\left(t_{Dus}\right)\right)^2+G\times\ln\left(\left(t_D*P_D'\right)_{us}\right)} \quad (16)$$

With constants depending on λ_{mf}, λ_{mv}, ω_f and ω_v values given in Table-11.

9) Another way of using the Equation (16) and taking into account the development for Equations (9) and (10); then, Equation (16) can be rewritten as:

$$\lambda_{vf}=\frac{A+B\times\ln\left(t_{Dusi}\right)+C\times\left(\ln\left(t_{Dusi}\right)\right)^2}{D+E\times\ln\left(t_{Dusi}\right)+F\times\left(\ln\left(t_{Dusi}\right)\right)^2} \quad (17)$$

Table-11. Constants for Equation (16).

Rank λ_{vf}	1×10^{-9} to 1×10^{-7}	5×10^{-7} to 1×10^{-5}
λ_{mf}	1×10^{-2}	1×10^{-1}
λ_{mv}	1×10^{-8}	1×10^{-7}
ω_f	1×10^{-2}	1×10^{-1}
ω_v	1×10^{-3}	1×10^{-2}
A	9.473719×10^{-9}	-2.3554034×10^{-6}
B	-1.9452657×10^{-9}	6.2511182×10^{-7}
C	1.0186085×10^{-10}	-4.1006933×10^{-8}
D	6.5972841×10^{-11}	6.9129679×10^{-9}
E	-0.21933576	-0.29487292
F	0.012033019	0.021752823
G	-0.0010661593	0.0011396252

With its constants provided in Table-12.

Table-12. Constant for Equation (17)

Rank λ_{vf}	1×10^{-9} to 1×10^{-7}	5×10^{-7} to 1×10^{-5}
λ_{mf}	1×10^{-2}	1×10^{-1}
λ_{mv}	1×10^{-8}	1×10^{-7}
ω_f	1×10^{-2}	1×10^{-1}
ω_v	1×10^{-3}	1×10^{-2}
A	9.42799011×10^{-9}	-2.3601951×10^{-6}
B	-1.9452657×10^{-9}	6.2511182×10^{-7}
C	1.0186085×10^{-10}	-4.1006933×10^{-8}
D	1.000739005	0.999210072
E	-0.21933576	-0.29487292
F	0.012033019	0.021752823

2.4. Dimensionless fracture storativity coefficient, ω_f

The same analysis and aspects that were considered in the study of interporosity flow parameters are used for the dimensionless storativity coefficients. Basically, the effect on the dimensionless pressure derivative due to variation of dimensionless storativity coefficients depends upon the size of the transition periods (size of the depression).

In the same fashion as for λ_{mv}, the starting time of the second radial flow regime converges at the same point for different ω_f values and the unit-slope line during the transition period varies in length but in terms of location is the same (no parallel displacement occurs along the time axis). The developed correlations for the calculation of the dimensionless fracture storativity coefficient are presented.

10) Using the second minimum point, $P_{Dmin2}/(t_D*P_D')_{min2}$ and t_{Dmin2}:

$$\omega_f=\frac{A+\left(B\times\ln\left(t_{D\min2}\right)\right)+\left(C\times\left(\frac{P_{D\min2}}{\left(t_D*P_D'\right)_{\min2}}\right)\right)}{1+\left(D\times\ln\left(t_{D\min2}\right)\right)+\left(E\times\left(\frac{P_{D\min}}{\left(t_D*P_D'\right)_{\min2}}\right)\right)} \quad (18)$$

For the range of $1\times10^{-3}<\omega_f<1\times10^{-2}$ the constants are provided in Table-13 and for $1\times10^{-2}<\omega_f<1\times10^{-1}$ the constants are given in Table-14.

11) Using the dimensionless vugs storativity coefficient and the second minimum point, $t_{Dmin2}*(t_D*P_D')_{min2}$:

$$\omega_f=\frac{A+B\times Z+C\times Z^2+D\times Z^3+\left(E\times\omega_v\right)}{1+F\times Z+(G\times\omega_v)+(H\times\omega_v^2)+(I\times\omega_v^3)} \quad (19)$$

being Z the product $t_{Dmin2}*(t_D*P_D')_{min2}$

Table-13. Constants for Equation (18).

λ_{vf}	1×10^{-10}	1×10^{-9}	1×10^{-8}
λ_{mv}	1×10^{-13}	1×10^{-12}	1×10^{-11}
λ_{mf}	1×10^{-7}	1×10^{-6}	1×10^{-5}
ω_v	1×10^{-7}	1×10^{-6}	1×10^{-5}
A	-0.001704	-0.00972031	0.006821921
B	-0.00037989	0.000383259	-0.00026108
C	2.83459×10^{-06}	6.25012×10^{-06}	-0.000027956
D	-0.06035366	-0.07376984	-0.09143191
E	-0.00275305	-0.00230932	4.51481×10^{-05}

Table-14. Constants for Equation (18).

λ_{vf}	1×10^{-6}	1×10^{-7}	1×10^{-8}	1×10^{-9}	1×10^{-10}
λ_{mv}	1×10^{-9}	1×10^{-10}	1×10^{-11}	1×10^{-12}	1×10^{-13}
λ_{mf}	1×10^{-3}	1×10^{-4}	1×10^{-5}	1×10^{-6}	1×10^{-7}
ω_v	1×10^{-4}	1×10^{-4}	1×10^{-5}	1×10^{-6}	1×10^{-7}
A	-0.1954122	1.08574413	0.563443198	0.025335109	0.031881466
B	-0.10102445	-0.0694529	-0.05643964	-0.00389316	-0.00352166
C	0.2754074	-0.0173495	-0.0002592	1.21575×10^{-05}	2.55978×10^{-06}
D	0.0363188	-0.1278309	-0.07562235	-0.0641791	-0.0559242
E	-0.7619847	0.05136569	-0.01871387	-0.00854222	-0.00647706

For the range of $1\times10^{-2} < \omega_f < 1\times10^{-1}$ the constants for Equation (19) are shown in Table-15.

Table-15. Constants for Equation (19).

λ_{vf}	1×10^{-6}	1×10^{-7}	1×10^{-8}
λ_{mv}	1×10^{-9}	1×10^{-10}	1×10^{-11}
λ_{mf}	1×10^{-3}	1×10^{-4}	1×10^{-5}
ω_v	1×10^{-4} a 1×10^{-5}	1×10^{-4} a 1×10^{-5}	1×10^{-4} a 1×10^{-5}
A	0.008088891	0.009042676	0.009173307
B	0.001645593	0.000166906	1.67034×10^{-05}
C	-5.2357×10^{-06}	-5.7774×10^{-08}	-5.8567×10^{-10}
D	2.62323×10^{-08}	2.91282×10^{-11}	2.97594×10^{-14}
E	-1678.67637	-1639.2486	-1637.05428
F	0.003283867	0.000319506	3.29846×10^{-05}
G	-10161.9333	-12050.8585	-13037.4575
H	34220600	92257700	106184000
I	2.27831×10^{11}	-1.4116×10^{11}	-2.3217×10^{11}

Table-16. Constants for Equation (20).

λ_{vf}	1×10^{-6}	1×10^{-7}	1×10^{-8}	1×10^{-9}
λ_{mv}	1×10^{-9}	1×10^{-10}	1×10^{-11}	1×10^{-12}
λ_{mf}	1×10^{-3}	1×10^{-4}	1×10^{-5}	1×10^{-6}
ω_f	1×10^{-3}	1×10^{-4}	1×10^{-5}	1×10^{-6}
A	-1.2604×10^{-06}	-6.4072×10^{-07}	-5.507×10^{-07}	-6.0548×10^{-07}
B	-2.8684×10^{-08}	-3.092×10^{-09}	-4.7228×10^{-10}	-3.327×10^{-11}
C	2.53119×10^{-10}	2.81413×10^{-12}	2.62234×10^{-14}	2.60903×10^{-16}
D	0.000281329	0.000283662	0.000342072	0.000295697
E	0.004368705	0.000474133	4.24526×10^{-05}	4.43181×10^{-06}
F	-1.1735×10^{-06}	-1.3626×10^{-08}	-1.2531×10^{-10}	-1.222×10^{-12}
G	-10.5345235	-10.8263553	-9.74235409	-10.449659

13) Using the beginning the second radial flow, t_{Db2}:

$$\omega_v = A + Bt_{Db2} + Ct_{Db2}^{1.5} + Dt_{Db2}^2 + Et_{Db2}^2 \ln(t_{Db2}) \qquad (21)$$

The above expression applies for $1\times10^{-2} < \omega_f < 1\times10^{-1}$ and its constants are given in Table-17.

2.5. Dimensionless Vugs Storativity Coefficient, ω_v

Unlike the observations for ω_f, the starting time of the second radial flow regime does not converge at the same point for different ω_v values, and unit-slope line of the transition period varies in length and in location. These considerations are used for the development of the correlations.

Table-17. Constant for Equation (22).

λ_{vf}	1×10^{-5}	1×10^{-6}	1×10^{-7}	1×10^{-8}	1×10^{-9}
λ_{mv}	1×10^{-8}	1×10^{-9}	1×10^{-10}	1×10^{-11}	1×10^{-12}
λ_{mf}	1×10^{-2}	1×10^{-3}	1×10^{-4}	1×10^{-5}	1×10^{-6}
ω_f	1×10^{-2}	1×10^{-3}	1×10^{-4}	1×10^{-5}	1×10^{-6}
A	0.007676832	6.14386×10^{-05}	-0.00028323	-0.00047454	-0.00041341
B	-1.9204×10^{-06}	1.79456×10^{-07}	1.91542×10^{-08}	2.1017×10^{-09}	1.97731×10^{-10}
C	2.5944×10^{-08}	-8.8781×10^{-12}	-2.2493×10^{-13}	-7.9535×10^{-14}	-8.155×10^{-16}
D	-1.8222×10^{-10}	6.99042×10^{-14}	3.34262×10^{-17}	3.17546×10^{-17}	9.03711×10^{-20}
E	1.15661×10^{-11}	-4.2625×10^{-15}	-6.4638×10^{-19}	-1.4331×10^{-18}	-3.6323×10^{-21}

12) Using the second minimum point, $(t_D*P_D')_{min2}$ and t_{Dmin2}:

$$\omega_v = \frac{A+(B\times t_{D\min 2})+(C\times t_{D\min 2}^2)+D\times(t_D*P_D')_{\min 2}}{1+(B\times t_{D\min 2})+(F\times t_{D\min 2}^2)+G\times(t_D*P_D')_{\min 2}} \qquad (20)$$

Which applied for $1\times10^{-6} < \omega_f < 1\times10^{-4}$ with the constants given in Table-16.

3. EXAMPLES

To observe the results obtained by the proposed correlations, only two examples are presented for space-saving purposes. The first one is a synthetic case and second one corresponds to a pressure test of a naturally fractured reservoir offshore vuggy located in the southeast of Mexico presented by Camacho *et al.* (2005).

3.1. Synthetic example

Pressure and pressure derivative for this test is provided in Figure-8. Other relevant data are given in the second column of Table-18 and below:

$q = 210$ STB s = 0 $C = 0$ bbl/psi
$h = 160$ ft $c_t = 1.4\text{x}10^{-6}$ psi^{-1}
$r_w = 0.21$ ft $\phi = 37\%$ $\mu = 1.2$ cp
$k = 231$ md $B = 1.3$ bbl/STB

Solution. The following information was read from Figure-8.

t_{min2}	6.2×10^{-4} hr	$(t*\Delta P')_{us}$	0.41 psi
ΔP_{min2}	6.4 psi	t_{usi}	9.8×10^{-3} hr
$(t*\Delta P')_{min2}$	0.05 psi	t_{b2}	0.048 hr
t_{us}	6.2×10^{-3} hr	Δt_D	0.00918 hr

Although, in the original work of Rojas and Rojas (2014) the naturally-fractured parameters were estimated several times from different for space-saving purposes only one estimation will be provided. Using the second minimum point, P_{Dmin2}/ $(t_D*P_D')_{min2}$ and t_{Dmin2}, λ_{mf} is calculated with Equation (4) and λ_{vf} is calculated with Equation (13). For λ_{mv} was estimated with Equation (9) by using the point between of intersection between the unit-slope line with the the second radial flow regime extrapolated line, t_{Dusi}. In order to calculate ω_v a point during the unit-slope line is read and replaced into Equation (15). Finally, ω_f is calculated with Equation (14) which uses the second lowest or minimum point on the pressure derivative curves. Needless to say that the readings from the plot are in oil-field units and they need to be translated to their dimensionless form. The results and its comparison with the actual parameters are given in Table-18.

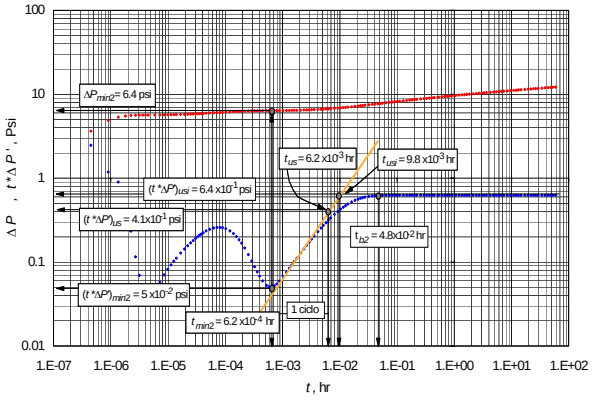

Figure-8. Pressure and pressure derivative versus time for example-1.

Table-18. Results for the synthetic example

Parameters	Actual	This study	Equation
λ_{mf}	1×10^{-4}	9.8537×10^{-5}	4
λ_{mv}	1×10^{-10}	1.18034×10^{-12}	11
λ_{vf}	1×10^{-7}	1.03007×10^{-7}	15
ω_f	1×10^{-4}	1.839317×10^{-3}	19
ω_v	1×10^{-5}	9.85352×10^{-6}	20

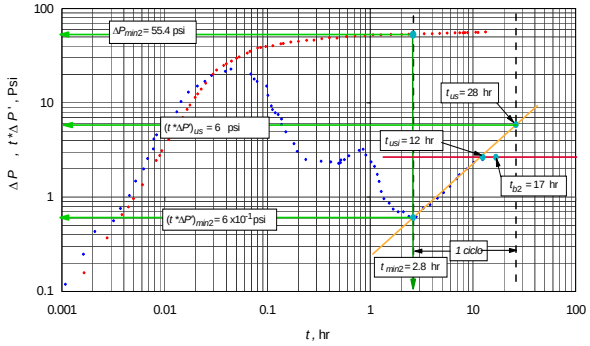

Figure-9. Points read from the pressure test for a field southeast of Mexico presented in the work of Camacho *et al.* (2005).

3.2. Field example

Camacho *et al.* (2005) presented a well test from an offshore naturally fractured vuggy reservoir located in southwestern Mexico. The test was digitized from Camacho *et al.* (2005) and reported in Figure-9. This field is an anticline affected by a normal fault, parallel to the major axis of the structure. This fact facilitated the saline intrusion at the middle of the field, dividing it into two blocks. The well was completed in a Cretaceous formation with a thickness between 170 to 278 meters. Other information is given below:

$q = 75$ STB $s = 2$ $C_D = 4500$
$h = 912.07$ ft $c_t = 1.4\text{x}10^{-6}$ psi^{-1} (assumed)
$r_w = 0.21$ ft $\phi = 40$ % $\mu = 0.6$ cp
$k = 524$ md

Solution. The following information was read from Figure-9.

t_{min2}	2.8 hr	$(t*\Delta P')_{us}$	6 psi
ΔP_{min2}	55.4 psi	t_{usi}	12 hr
$(t*\Delta P')_{min2}$	0.6 psi	t_{b2}	17 hr
t_{us}	28 hr	Δt_D	9 hr

Similar to the previous example, the data read from Figure-9 was converted into dimensionless form: $P_{Dmin2}/ (t_D*P_D')_{min2}$, t_{Dmin2} and t_{Dusi} with which the results reported in Table-19 are obtained.

Table-19. Results for field case.

Parameters	Equation	This work	Camacho *et al.* (2005)
λ_{mf}	4	8.425×10^{-5}	1×10^{-7}
λ_{mv}	12	1.1454×10^{-13}	1×10^{-8}
λ_{vf}	14	4.27×10^{-6}	1×10^{-5}
ω_f	18	7.3738×10^{-3}	1×10^{-3}
ω_v	21	8.781×10^{-3}	0.2

Although, in some cases the results differ in an order of magnitude with the actual values, the authors believe that the results are acceptable. Even though, for the field case, it was necessary to assume the system compressibility since it was not provided.

4. CONCLUSIONS AND RECOMMENDATIONS

New mathematical expressions based on the derived dimensionless pressure and dimensionless pressures for naturally fractured reservoir characterization vugulares during pseudosteady flow transition are formulated.

The effect of interporosity flow parameters and dimensionless storativity of vugs, matrix and fractures affect the transient-pressure; however, sometimes this is so small that cannot be correlated with the variation of the characteristic parameters.

The application of the developed expressions is sensitive to the accuracy of reading the characteristic points so they should be performed with an accuracy of at least two or three significant figures to reduce the error.

ACKNOWLEDGEMENTS

The authors gratefully thank the Most Holy Trinity and the Virgin Mary mother of God for all the blessing received during their lives.

Nomenclature

B	Volumetric factor, rb/STB
C	Storage coefficient, bbl/psi
C_A	Total compressibility, 1/psi
h	Formation thickness, ft
k	Permeability, md
q	Flow rate , STB/D
t	Time, hr
r	Radius, ft
S	Skin
$t*\Delta P'$	Pressure derivative, psi
t_D*P_D'	Derivative of the dimensionless pressure psi/BPD
P	Pressure, psi
P_D	Dimensionless pressure

Greeks

Δ	Change, drop
ϕ	Porosity, fraction
μ	Viscosity, cp
λ	Storage coefficient
ω	Interporosity flow parameter

Suffices

D	Dimensionless
min	First minimum
min2	Second minimum
us	Unitary slope
usi	Intercept between unitary slope and the second radial flow
r2	Second radial
b2	beginning second radial
f	Fractures
v	Vugs
mf	Matrix-fractures
mv	Matrix-vugs
vf	Vugs-fractures

Appendix-A. Mathematical model proposed by Camacho-Velazquez *et al*. (2005).

The dimensionless partial differential equation for cylindrical geometry is given by,

$$\frac{1}{r_D}\frac{\partial}{\partial r_D}\left(r_D\frac{\partial P_{Df}}{\partial r_D}\right)+\lambda_{mf}\left(P_{Dm}-P_{Df}\right)+\lambda_{vf}\left(P_{Dv}-P_{Df}\right)=\omega_f\frac{\partial P_{Df}}{\partial t_D} \quad (A.1)$$

Fort the matrix blocks and vugs the governing equations, respectively, are:

$$-\lambda_{mv}\left(P_{Dm}-P_{Dv}\right)-\lambda_{mf}\left(P_{Dm}-P_{Df}\right)=\left(1-\omega_f-\omega_v\right)\frac{\partial P_{Dm}}{\partial t_D} \quad (2.2)$$

$$\lambda_{mv}\left(P_{Dm}-P_{Dv}\right)-\lambda_{vf}\left(P_{Dv}-P_{Df}\right)=\omega_v\frac{\partial P_{Dv}}{\partial t_D} \quad (A.3)$$

Where the dimensionless quantities are given by:

$$P_{Dj}=\frac{2\pi k_f h\left(P_i-P_j\right)}{q\mu B} \quad (A.4)$$

Being *j* = fractures o vugs, and,

$$t_D=\frac{k_f t}{\left[\left(\phi_f c_f+\phi_m c_m+\phi_v c_v\right)\mu r_w^2\right]} \quad (A.5)$$

The interporosity flow parameters are defined below:

$$\lambda_{mf}=\frac{\sigma_{mf}k_m r_w^2}{k_f} \quad (A.6)$$

$$\lambda_{mv}=\frac{\sigma_{mv}k_m r_w^2}{k_f} \quad (A.7)$$

$$\lambda_{vf}=\frac{\sigma_{vf}k_{vf} r_w^2}{k_f+k_v} \quad (A.8)$$

Where $k_{vf}=k_v$ if $P_v>P_f$ and $k_{vf}=k_f$ if the contrary case. σ *i*s the shape factor between the media "*i*" and "*j*". The dimensionless storativity coefficients are given as:

$$\omega_f=\frac{\phi_f c_f}{\phi_f c_f+\phi_m c_m+\phi_v c_v} \quad (A.9)$$

$$\omega_v=\frac{\phi_v c_v}{\phi_f c_f+\phi_m c_m+\phi_v c_v} \quad (A.10)$$

For the constant wellbore pressure condition, the dimensionless flow rate is defined by:

$$q_{wD}=\frac{q\mu B}{2\pi h\left(k_f+k_v\right)\left(P_i-P_{wf}\right)} \quad (A.11)$$

Camacho-Velazquez *et al*. (2005) found the Laplace pressure solutions as;

$$\overline{P_{DV}}=\overline{P_{DV}}\left[\left(b_1+b_2u\right)/\left(b_3+b_4u+b_5u^2\right)\right] \quad (A.12)$$

where,

$$b_1=\lambda_{vf}\left(\lambda_{mv}+\lambda_{mf}\right)+\lambda_{mf}\lambda_{mv} \quad (A.13)$$

$$b_2=\lambda_{vf}\left(1-\omega_f-\omega_v\right) \quad (A.14)$$

$$b_3=\lambda_{mv}\left(\lambda_{vf}+\lambda_{mf}\right)+\lambda_{mf}\lambda_{vf} \quad (A.15)$$

$$b_4=\omega_v\left(\lambda_{mv}+\lambda_{mf}\right)+\left(1-\omega_f-\omega_v\right)\left(\lambda_{mv}+\lambda_{vf}\right) \quad (A.16)$$

$$b_5=\left(1-\omega_f-\omega_v\right)\omega_v \quad (A.17)$$

$$\overline{P_{Dm}}=\overline{P_{Df}}\left(\frac{c_1+uc_2+u^2c_3}{d_1+ud_2+u^2d_3+u^3d_4}\right) \quad (A.18)$$

where,

$$c_1=\lambda_{mv}b_1+\lambda_{mf}b_3 \quad (A.19)$$

$$c_2=\lambda_{mv}b_2+\lambda_{mf}b_4 \quad (A.20)$$

$$c_3=\lambda_{mf}b_5 \quad (A.21)$$

$$d_1=\left(\lambda_{mv}+\lambda_{mf}\right)b_3 \quad (A.22)$$

$$d_2 = (\lambda_{mv} + \lambda_{mf})b_4 + (1 - \omega_f - \omega_v)b_3 \quad \text{(A.23)}$$

$$d_3 = (\lambda_{mv} + \lambda_{mf})b_5 + (1 - \omega_f - \omega_v)b_4 \quad \text{(A.24)}$$

and,

$$d_4 = (1 - \omega_f - \omega_v)b_5 \quad \text{(A.25)}$$

Since the internal condition is set as constant flow rate and considering skin and wellbore storage effects, the final solution for an infinite reservoir as presented by Camacho-Velazquez *et al*. (2005) is:

$$\overline{P_{wD}} = \frac{K_0\left[\sqrt{g(u)}\right] + s\sqrt{g(u)}K_1\left[\sqrt{g(u)}\right]}{u\left(\sqrt{g(u)}K_1\left[\sqrt{g(u)}\right] + C_D u\left\{K_0\left[\sqrt{g(u)}\right] + s\sqrt{g(u)}K_1\left[\sqrt{g(u)}\right]\right\}\right)} \quad \text{(A.26)}$$

where,

$$\begin{aligned} g(u) = {} & \lambda_{mf}(1 - [\lambda_{mv}b_1\lambda_{mf}b_3 + u(\lambda_{mv}b_2 + \lambda_{mf}b_4) + \\ & u^2\lambda_{mf}b_5 / \{b_3(\lambda_{mv} + \lambda_{mf}) + u[(\lambda_{mv} + \lambda_{mf})b_4 + \\ & (1 - \omega_f - \omega_v)b_3] + u^2[(\lambda_{mv} + \lambda_{mf})b_5 + (1 - \omega_f - \omega_v)b_4] + \\ & u^3(1 - \omega_f - \omega_v)b_5\}]) + \lambda_{mf}\left(1 - \frac{b_1 + b_2 u}{b_3 + b_4 u + b_5 u^2}\right) + \omega_f u \end{aligned} \quad \text{(A.27)}$$

REFERENCES

Abdassah D. and Ershaghi I. 1986. Triple-Porosity Systems for Representing Naturally Fractured Reservoirs. SPEFE (April 1986) 113; Trans., AIME, 281.

Barenblatt G.I., Zheltov I.P. and y Kochina I.N. 1960. Basic Concepts in the Theory of Seepage of Homogenous Liquid in Fissured Rocks. PMM, Sov. Appl. Math. Mech. pp. 24-25.

Camacho R., *et al*. 2005. Pressure-Transient and Decline-Curve Behavior in Naturally Fractured Vuggy Carbonate Reservoirs. Paper SPE 77689.

Camacho-Velazquez R., Vazquez-Cruz M., Castejón-Alvar R. and Arana-Ortiz V. 2005. Pressure-Transient and Decline-Curve Behavior in Naturally Fractured Vuggy Carbonate Reservoirs. SPE Formation Evaluation & Engineering. pp. 95-111. April.

Escobar F.H., Saavedra N.F., Escorcia G.D. and Polanía J.H. 2004. Pressure and Pressure Derivative Analysis Without Type-Curve Matching for Triple Porosity Reservoirs. Paper SPE 88556, memorias, Conference and Exhibition of the SPE, about Oil and Gas Asia Pacific (APOGCE), in Perth, Australia. October 18-20.

Neale G.H. and Nader W.K. 1973. The Permeability of a Uniformly Vuggy Porous Medium. SPEJ, April.

Mirshekari B., Modarress H. and Hamzehnataj E. 2007. Application of Pressure Derivative Function for well test Analysis of Triple Porosity SNaturally ractured Reservoirs. Society of Petroleum Engineers. doi:10.2118/110943-MS.

Rojas J.D. and Rojas R.F. 2014. Análisis de Presión y Derivada de Presión para Yacimientos de Triple Porosidad y Unica Permeabilidad en Yacimientos Naturalmente Fracturados y Vugulares. Universidad Surcolombiana. (Neiva-Huila-Colombia). B.S. Thesis.

Rodriguez F., Arana O.V. and Cinco L. H. 2004. Well Test Characterization of Small and Large Scale Secondary Porosity in Naturally Fractured Reservoirs. Paper SPE 90287.

Tiab D. 1993. Analysis of Pressure and Pressure Derivative without Type-Curve Matching: 1- Skin and Wellbore Storage. Journal of Petroleum Science and Engineering. 12: 171-181.

Warren J.E. and Root P.J. 1963. The Behavior of Naturally Fractured Reservoirs. SPEJ, September. pp. 245-255.

Wu Y. S. and Cols. 2004. A Triple-Continuum Approach for Modeling Flow and Transport Processes in Fractured Rock. Journal of Contaminant Hydrology, Elsevier, January.